

Control of G protein-coupled receptor function via membrane-interacting intrinsically disordered C-terminal domains

Chiara D. Mancinelli^{a,1} 🗓, Dagan C. Marx^{a,1}, Alberto J. Gonzalez-Hernandez^{a,1}, Kevin Huynh^a, Lucia Mancinelli^a, Anisul Arefin^a, George Khelashvilli^b 🗓, Joshua Levitz^{a,c,2}, and David Eliezer^{a,d,2}

Affiliations are included on p. 11.

Edited by Scott R. Prosser, University of Toronto, Mississauga, ON, Canada; received April 29, 2024; accepted June 7, 2024 by Editorial Board Member Robert J. Lefkowitz

G protein-coupled receptors (GPCRs) control intracellular signaling cascades via agonist-dependent coupling to intracellular transducers including heterotrimeric G proteins, GPCR kinases (GRKs), and arrestins. In addition to their critical interactions with the transmembrane core of active GPCRs, all three classes of transducers have also been reported to interact with receptor C-terminal domains (CTDs). An underexplored aspect of GPCR CTDs is their possible role as lipid sensors given their proximity to the membrane. CTD-membrane interactions have the potential to control the accessibility of key regulatory CTD residues to downstream effectors and transducers. Here, we report that the CTDs of two closely related family C GPCRs, metabotropic glutamate receptor 2 (mGluR2) and mGluR3, bind to membranes and that this interaction can regulate receptor function. We first characterize CTD structure with NMR spectroscopy, revealing lipid composition-dependent modes of membrane binding. Using molecular dynamics simulations and structure-guided mutagenesis, we then identify key conserved residues and cancer-associated mutations that modulate CTD-membrane binding. Finally, we provide evidence that mGluR3 transducer coupling is controlled by CTD-membrane interactions in live cells, which may be subject to regulation by CTD phosphorylation and changes in membrane composition. This work reveals an additional mechanism of GPCR modulation, suggesting that CTD-membrane binding may be a general regulatory mode throughout the broad GPCR superfamily.

GPCR | mGluR | β-arrestin | NMR | disordered protein

G protein-coupled receptors (GPCRs) respond to extracellular stimuli to drive intracellular signal transduction pathways that control a wide variety of biological functions. Consistent with their widespread physiological roles, GPCRs also serve as a major class of targets for disease intervention (1, 2). All GPCRs share a conserved architecture including an N-terminal extracellular domain (ECD) of variable size, a seven-helix transmembrane domain (TMD) and an intracellular C-terminal domain (CTD). Signaling is initiated by binding of extracellular ligands to the receptor ECD and/or TMD, inducing conformational changes that control coupling of receptor TMD and CTD to intracellular transducers, including heterotrimeric G proteins, GPCR kinases (GRKs), and β-arrestins (β-arrs).

GPCR CTDs typically feature low sequence complexity, are absent from most structures determined by X-ray crystallography or cryo-EM, and usually lack secondary structure in sequence-based predictions, including AlphaFold, suggesting that they are, in general, highly dynamic. Indeed, several recent studies of isolated or unbound GPCR CTDs have shown that they are intrinsically disordered (3–6). Well-defined GPCR CTD conformations have been captured at high resolution in only a handful of complexes that feature CTD-G protein (7-10) or CTD-arrestin (11-17) interactions and are typically limited to small segments. In addition to their roles in direct interaction with transducers, the proximity of GPCR CTDs to the membrane may also promote direct interactions with phospholipids. Indeed, membrane binding has been observed for the isolated CTD of the cannabinoid receptor 1 (18), and many GPCR CTDs are palmitoylated (19), but the functional implications of CTD-membrane interactions are unclear. CTD-membrane interactions could influence receptor interactions and conformation and thereby modulate receptor-ligand binding, activation, and trafficking. Furthermore, such interactions could be sensitive to lipid composition, providing one

Significance

G protein-coupled receptors (GPCRs) allow cells to sense and respond to their environment and constitute the largest class of targets for approved therapeutic drugs. Temporally precise GPCR signaling is achieved by allosterically coupling the binding of extracellular ligands to intracellular signal transducers (e.g., heterotrimeric G proteins) and regulators (e.g., β-arrestins). The C-terminal domains (CTDs) of GPCRs are targets of posttranslational modifications and play a critical role in transducer and regulator recruitment. Here, we report interactions of the CTDs of two GPCRs of the metabotropic glutamate receptor family with cellular membranes. These interactions regulate CTD accessibility and thus, mGluR coupling to transducers and regulators. We propose that dynamic CTD-membrane interaction constitutes a general mechanism for regulating GPCR function.

Preprint Severs: This article was deposited as a preprint in bioRxiv under a CC BY-NC-ND license

The authors declare no competing interest.

This article is a PNAS Direct Submission. S.R.P. is a guest editor invited by the Editorial Board.

Copyright © 2024 the Author(s). Published by PNAS. This article is distributed under Creative Commons Attribution-NonCommercial-NoDerivatives License 4.0 (CC BY-NC-ND).

¹C.D.M., D.C.M., and A.J.G.-H. contributed equally to this work. ²To whom correspondence may be addressed. Email: jtl2003@med.cornell.edu or dae2005@med.cornell.edu.

This article contains supporting information online at https://www.pnas.org/lookup/suppl/doi:10.1073/pnas. 2407744121/-/DCSupplemental.

Published July 10, 2024.

avenue by which lipids could dynamically regulate receptor function. Along these lines, recent work has demonstrated that reconstituted GPCR activity can be tuned by interactions with specific lipids (20–22), and that β -arr can also directly interact with the lipid bilayer in its receptor-bound state (16, 23–25).

Metabotropic glutamate receptors (mGluRs) are dimeric, family C GPCRs that are characterized structurally by their large ECDs which contain a ligand binding domain (LBD) that senses the neurotransmitter glutamate and a cysteine-rich domain that connects the LBD to the TMD (Fig. 1A) (26). Despite this unique ECD arrangement, upon glutamate binding by the LBD, mGluRs couple to G proteins via their TMD in a manner generally analogous to, yet distinct in detail, from that of other GPCR families (9, 27-29). As with other GPCRs, the CTDs of mGluRs are known to be major determinants of their interactions with transducers and regulatory factors (30-33). Notably, we recently found that modest differences in CTD composition control the ability of the highly homologous group II mGluRs, mGluR2, and mGluR3, to recruit β-arrs (34). mGluR3 is efficiently phosphorylated by GRKs and recruits β -arr, which initiates clathrin-mediated receptor endocytosis, while mGluR2 largely eludes β-arr-driven

internalization. This difference is encoded in a short ~20 residue serine/threonine (S/T) rich region of the CTD that begins ~15 residues after the end of TMD helix 7 (34).

The central role of the CTD in subtype-specific mGluR regulation raises the question of its structural properties and whether its proximity to the membrane may shape its structure or function. Despite recent cryo-EM studies which have resolved the structures of mGluR ECDs and TMDs in inactive and active states (9, 29, 35–38), structural information on group II mGluR CTDs is limited to a short membrane-proximal segment of the mGluR2 CTD (residues 821 to 830) which was observed bound to G protein in a recent report (9). Here, we examine the structural properties and membrane interactions of the CTDs of mGluR2 and mGluR3. Using a combination of spectroscopic and computational approaches we find that both mGluR2 and mGluR3 CTDs are intrinsically disordered but are capable of interaction with phospholipid membranes. We show that both TMD-proximal and -distal basic residues can mediate electrostatic interactions with lipid headgroups. Additionally, we identify in mGluR3 an aromatic residue, Y853, that can partition into the membrane interface to potentially restrict access to the mGluR3 CTD S/T-rich region. We then find that

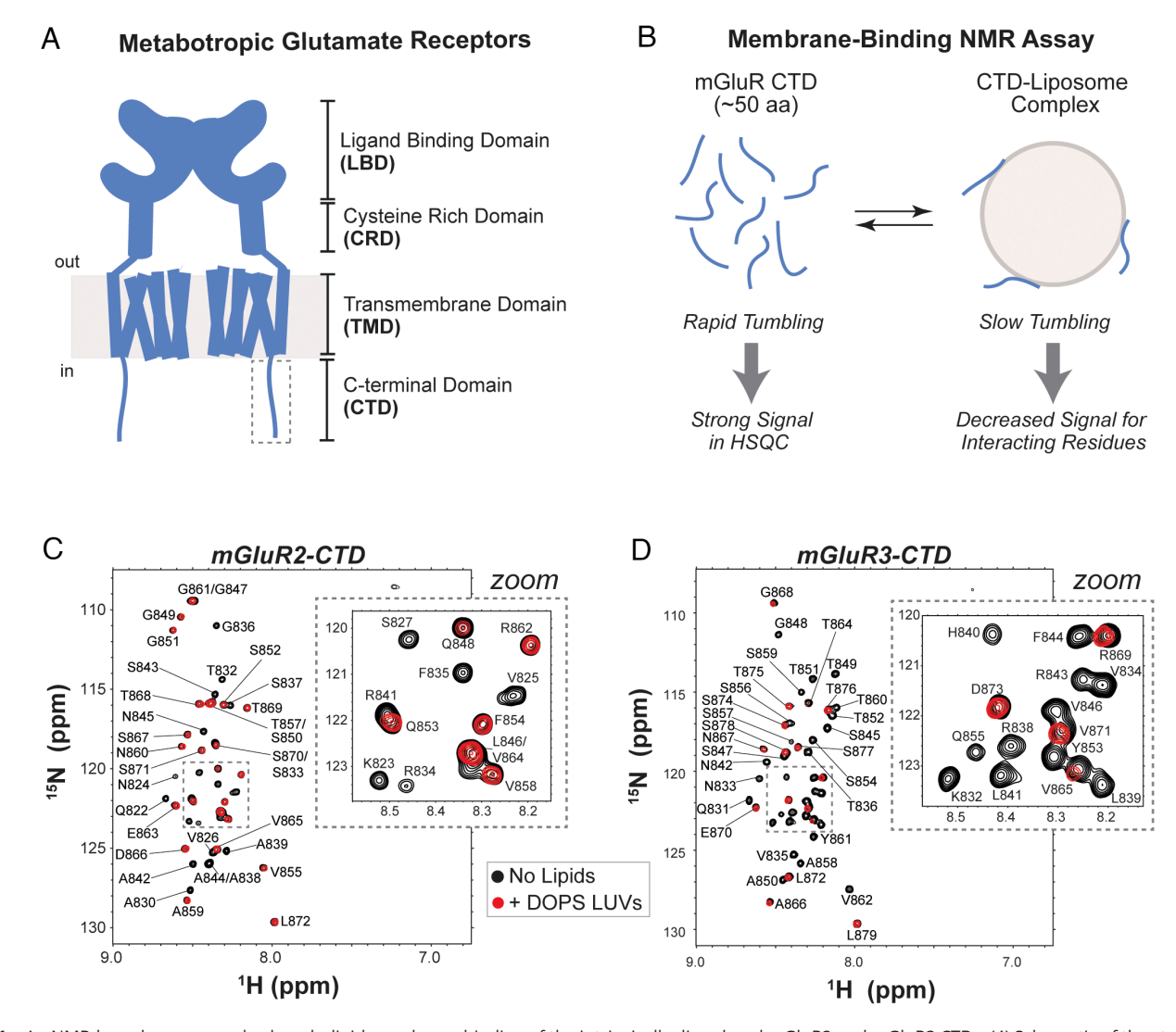


Fig. 1. An NMR-based assay reveals phospholipid membrane binding of the intrinsically disordered mGluR2 and mGluR3 CTDs. (*A*) Schematic of the structural organization of mGluR domains highlighting the location of the CTD compared to the ordered parts of the protein and the membrane. (*B*) Schematic of NMR-based CTD-membrane binding assay that takes advantage of changes in tumbling rates of the CTD due to interactions with large unilamellar vesicles (LUVs). (*C*) ¹H-¹⁵N HSQC spectra of isolated mGluR2* and (*D*) mGluR3* CTD in the presence (red) and absence (black) of 10 mM 100 nm diameter LUVs comprised DOPS at pH 6.8 at 10 °C, with zoomed insets of crowded regions, highlighting loss of signal of specific residues in the presence of LUVs.

point mutations, including those associated with melanoma, can modulate membrane interactions, β-arr-dependent internalization, and G protein activation in cells. Furthermore, we show that EGF stimulation leads to agonist-independent mGluR3 internalization, depending on the presence of Y853, suggesting that Y853 phosphorylation may drive receptor internalization by reducing binding of the CTD to the membrane. Together this work suggests complex and dynamic interactions between the intrinsically disordered CTD and the membrane, expanding the known repertoire of GPCR regulatory mechanisms.

Results

Disordered mGluR CTDs Bind Negatively Charged Membranes In Vitro. To investigate the structure of mGluR CTDs and probe potential membrane interactions, we turned to NMR spectroscopy using purified, recombinant CTD constructs. For a quantitative, single-residue resolution assay of membrane binding, we took advantage of the effects of the slow tumbling rates of LUVs on NMR signals. Briefly, interactions of intrinsically disordered proteins (IDPs) with vesicles attenuate the signals of residues that interact with the membrane because they adopt the slow tumbling rates and long rotational correlation times of the LUVs (Fig. 1*B*). This assay has been used extensively to characterize IDP/membrane interactions (39-41) but has not been applied to GPCR CTDs. We first obtained 2D ¹⁵N-¹H HSQC spectra for both mGluR2 and mGluR3 CTDs in the absence of lipids, which exhibited the sharp signals and limited dispersion that are characteristic of IDPs (Fig. 1 C and D). In the presence of LUVs composed of DOPS (18:1 1,2-dioleoyl-sn-glycero-3-phospho-L-serine) many signals in the spectra of both CTDs were clearly attenuated (Fig. 1 C and D, Insets), indicative of an interaction between the corresponding CTD residues and the negatively charged vesicles. Spectra acquired in the presence of LUVs composed of 1:1 DOPS:DOPC (18:1 [Δ 9-Cis] 1,2-dioleoyl-sn-glycero-3-phosphocholine) or only DOPC exhibited variable degrees of signal loss (SI Appendix, Fig. S1) suggesting that CTD-membrane interactions are sensitive to lipid composition.

We then asked whether the mGluR CTDs form helical secondary structure upon membrane binding using circular dichroism (CD) spectroscopy. CD spectra of the mGluR2 (SI Appendix, Fig. S2A) and mGluR3 (SI Appendix, Fig. S2B) CTDs showed no evidence for alpha-helix formation either in the absence of lipids or in the presence of vesicles under conditions where maximal membrane binding was observed by NMR. Because formation of short segments of helical structure can be difficult to detect in longer polypeptides, we also examined CD spectra of shorter mGluR2 and mGluR3 CTD peptides corresponding more closely to just their membranebinding regions (Methods). These spectra (SI Appendix, Fig. S2 C and D) also showed no evidence of alpha-helix formation in the absence or presence of membranes. Even the presence of membrane mimetic SDS and DPC micelles, which often induce helical structure (42–44), did not result in helix formation (SI Appendix, Fig. S2E). As a control, we confirmed using CD that LUVs induce robust helical structure in a helix-8 peptide from NTS1 (SI Appendix, Fig. S2F), as previously reported (45). These results are consistent with the physicochemical characteristics of the membrane-binding regions of the mGluR2 and mGluR3 CTDs, which do not show the amphipathic nature typical of membrane-induced helices (see helical wheel plots in SI Appendix, Fig. S2 G and H) as well as with secondary structure predictions. Thus, it appears that the conformational ensemble sampled by group II mGluR CTDs upon membrane binding lacks persistent secondary structure and maintains a high degree of disorder.

Electrostatics Mediate mGluR CTD-Membrane Interactions. To enable sequence-specific analysis of CTD-membrane binding, we obtained NMR backbone resonance assignments using conventional triple resonance NMR experiments (Fig. 1 and SI Appendix, Fig. S1). Chemical shift-based secondary structure assessments confirmed the highly disordered nature of both CTDs in the absence of LUVs, as indicated by the lack of any significant secondary shifts (SI Appendix, Fig. S3 A and B) and corroborated using CheSPI (46), which indicated negligible probabilities for helix or strand secondary structure. Plots of the ratio of NMR signal intensities in the presence versus absence of LUVs as a function of position (Fig. 2 A and B) show that both mGluR CTDs interact with phospholipids via their N-terminal regions. For both CTDs, NMR signal attenuation is dependent on negatively charged lipid content, as signal attenuation is absent (mGluR2) or decreased (mGluR3) in the absence of DOPS (Fig. 2 A and B and SI Appendix, Fig. S1). Despite similar binding profiles at their N termini, the membrane-binding region for the mGluR3 CTD is longer, spanning the first ~30 residues, compared with ~21 residues for mGluR2. Plots of the average intensity ratio as a function of LUV composition within the N-terminal 20 residues (Fig. 2C) illustrate the clear DOPS dependence of membrane binding in this region, in contrast with the C-terminal region (Fig. 2D).

Inspection of the sequence of both mGluR CTDs revealed a conserved N-terminal cluster of basic residues (Fig. 3A), which we hypothesized could drive CTD binding to negatively charged DOPS headgroups. Mutation of each of the four basic residues in this cluster to alanine reduced membrane binding for this region of the mGluR2 CTD (Fig. 3 B–D and SI Appendix, Fig. S4), with the strongest effect observed for LUVs composed of 1:1 DOPS:DOPC, indicating that increasing negative charge content in the membrane can partly compensate for the loss of individual basic residues in the CTD (Fig. 3C). The strongest effect was observed for the R834A mutation, and mutation of the corresponding residue in mGluR3 to alanine (R843A) also lead to severe disruption of membrane binding by the mGluR3 CTD (Fig. 3E). These results support a major role for electrostatic interactions between basic CTD residues and anionic phospholipids in driving CTD-membrane interactions.

To further understand the properties of the mGluR CTDmembrane interaction, we examined the potential role of membrane curvature in altering the membrane-bound region of mGluR CTD. Notably, disordered protein segments can sense membrane curvature on short length scales by interacting with lipid packing defects, without the need for shape complementarity over longer distances (47, 48). We measured binding to DOPS vesicles with diameters ranging from 50-400 nm and observed no substantial changes in mGluR2 membrane binding, indicating that mGluR CTDs are insensitive to membrane curvature (SI Appendix, Fig. S5). To assess whether different regions of the protein bind to membranes with different affinities, we obtained NMR intensity ratio data for the mGluR3 CTD as a function of lipid concentration (SI Appendix, Fig. S6A). We found that the N-terminal basic cluster remains bound even at lower lipid concentrations but observed a reduction in binding of the subsequent residues (S845 to T860) comprising the S/T-rich region of the mGluR3 CTD, suggesting that this region binds less strongly (SI Appendix, Fig. S6C). To explore how CTD membrane interactions are affected by more complex lipid compositions that more closely resemble the plasma membrane inner leaflet, we measured mGluR3 CTD binding to DOPE-containing (1,2-dioleoyl-sn-glycero-3-phosphoethanolamine) vesicles composed of 11:4:5 DOPC:DOPE:DOPS with or without 30% cholesterol. The 25% negative charge content of these vesicles is similar

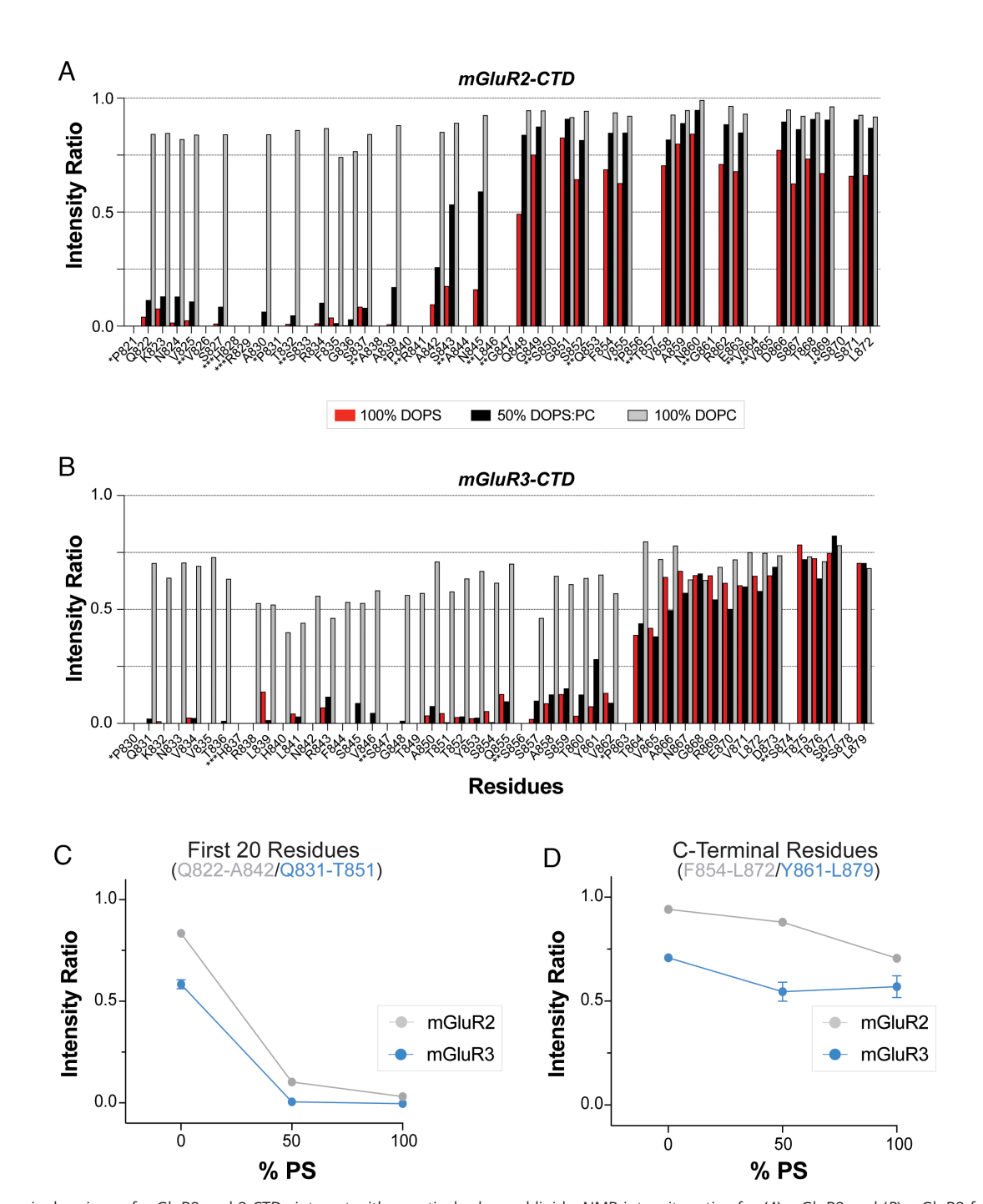


Fig. 2. N-terminal regions of mGluR2 and 3 CTDs interact with negatively charged lipids. NMR intensity ratios for (A) mGluR2 and (B) mGluR3 from spectra collected with and without LUVs of three different lipid compositions. Prolines, which do not give rise to signals in ¹H-¹⁵N HSQC spectra, are denoted by *, overlapping peaks for which values were not included by **, and residues not detected in the spectra by ***. (C) Averaged intensity ratios over the first ~20 residues (mGluR2 Q822-A842; mGluR3 Q831-T851) from (A) and (B) illustrate the lipid composition dependence of the interactions in this region (±SEM of this average). (D) Averaged intensity ratios over the last ~20 residues (mGluR2 Q853-L872; mGluR3 Y861-L879) from (A) and (B) illustrate the lack of lipid composition dependence of the interactions in this region (±SEM of this average).

to that expected for the inner leaflet of cellular plasma membranes (49, 50). The resulting binding profile (SI Appendix, Fig. S6A) exhibits strong binding in the basic cluster region, but attenuated binding in the S/T-rich region when compared with 1:1 DOPC: DOPS vesicles, consistent with reduced binding at lower negative charge content. Indeed, the profile closely resembles that observed in the presence of lower (2.5 mM) concentrations of 1:1 DOPC:DOPS vesicles (SI Appendix, Fig. S6A). The inclusion of 30% cholesterol did not alter the binding profiles, suggesting that cholesterol may not strongly influence CTD-membrane interactions (SI Appendix, Fig. S6A).

Finally, to assess CTD membrane binding in a concentrationindependent manner and in a context more closely resembling that of the intact membrane-inserted receptor, we anchored the mGluR3 CTD to vesicles by introducing a hexa-histidine tag at its N terminus and doping 5% DGS-Ni-NTA (1,2-dioleoyl-sn-glycero-3-[(N-(5amino-1-carboxypentyl) iminodiacetic acid)succinyl] (nickel salt)) into PC:PE:PS vesicles (10:4:5:1 DOPC:DOPE:DOPS:DGS-Ni-NTA). Intensity ratio plots for the anchored CTD revealed a signal attenuation profile consistent with that observed for the free CTD, with the strongest binding at the N terminus and clear, but decreasing binding through the S/T-rich and C-terminal regions (SI Appendix, Fig. S6E).

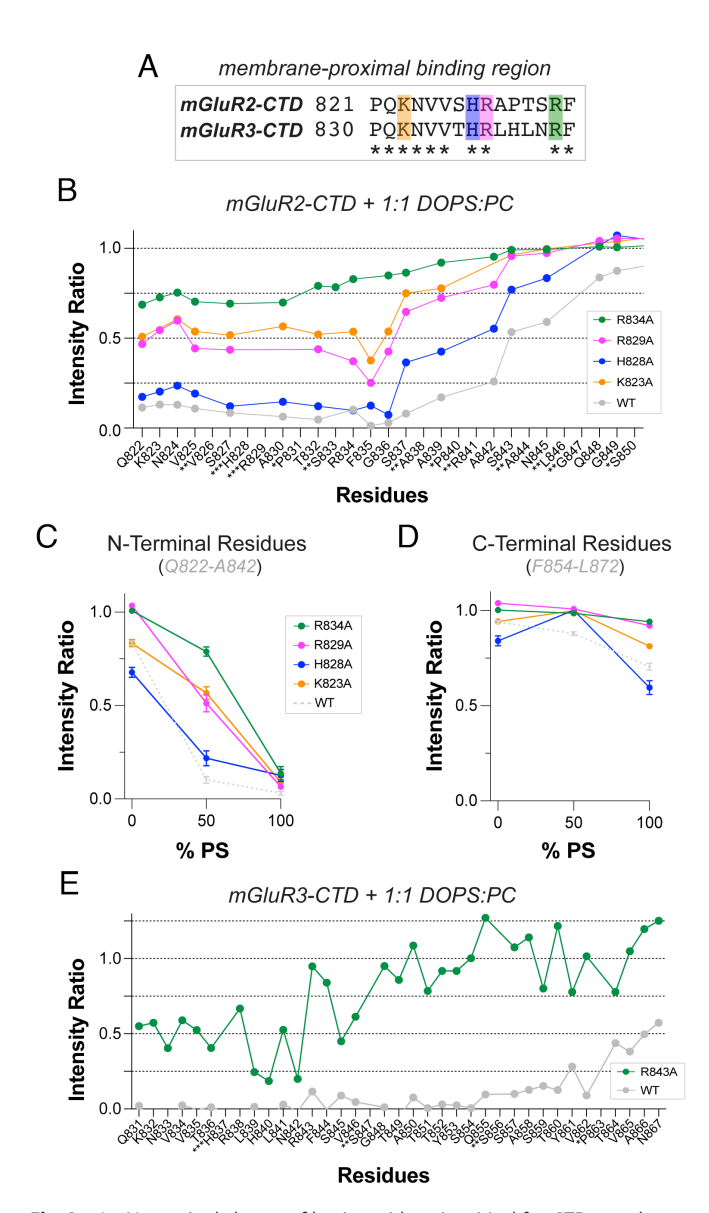


Fig. 3. An N-terminal cluster of basic residues is critical for CTD membrane binding. (A) sequence alignment of the first 15 residues of the mGluR2 and mGluR3 CTDs highlighting conserved (*) and positively charged (highlighted) residues. (B) Intensity ratio plots of mGluR2 CTD constructs containing alanine substitutions for each of the four basic residues from spectra collected with and without LUVs containing a 1:1 mixture of DOPS:DOPC lipids. (C) Averaged intensity ratios over the first ~20 residues (Q822-A842) from (B) illustrate the regional effect of each mutation for LUVs of different lipid composition (±SEM of this average). (D) Averaged intensity ratios over the last ~20 residues (Q853-L872) from (B) illustrate the regional effect of each mutation for LUVs of different lipid composition (±SEM of this average). (E) Intensity ratio plots of R843A mGluR3 CTD compared to WT from spectra collected with and without LUVs containing a 1:1 mixture of DOPS:DOPC lipids.

Importantly, the extent of attenuation for the anchored CTD is dramatically greater in the S/T-rich and C-terminal regions than that observed for the unanchored CTD using vesicles containing 50% negative charge content. Because nickel is paramagnetic, DGS-Ni-NTA will also induce some degree of paramagnetic relaxation enhancement (PRE) of CTD nuclei that approach within a ~25 Å distance, adding a distance-based signal attenuation to that resulting from immobilization of residues on the vesicle. To assess the extent of this effect, we measured intensity ratios for the unanchored CTD, lacking the N-terminal hexa-histidine tag, in the presence of DGS-Ni-NTA vesicles. This condition produced only minor broadening beyond that observed for corresponding vesicles lacking DGS-Ni-NTA, suggesting that NMR attenuation induced by slow tumbling upon membrane

binding dominates any DGS-Ni-NTA-associated PRE effects. Together, these results demonstrate that N-terminal anchoring of the mGluR3 CTD to vesicles results in enhanced membrane interactions, and indicate that the lipid concentrations and compositions and the sample conditions used in our in vitro studies of untethered CTD peptides do not result in artifactual binding profiles or overestimates of binding.

Aromatic and Distal Charged Residues Help Anchor the mGluR3 CTD S/T-Rich Region to the Membrane. To further probe structural changes in the mGluR CTDs upon binding to membranes, we turned to all-atom molecular dynamics simulations. We focused our analysis on the mGluR3 CTD, as this subtype features more extensive membrane interactions than mGluR2 (Fig. 2), and since the CTD is known to have a central role in mGluR3 regulation (34). We built a system containing a 1:1 DOPC/ DOPS phospholipid bilayer and a protein chain comprising both transmembrane helix 7 (TM7) of mGluR3 and the CTD (Methods). We included the transmembrane tether to increase the probability of observing CTD-membrane interactions within the simulation time and to bridge the in vitro experiments with isolated CTDs to the biological context of the CTD where it is attached to the TMD at its N terminus. We started the simulations with the CTD in a disordered conformation with no contacts with the membrane and 6 independent replicas were simulated for 1,370 ns each, resulting in 8.22 µs of total simulation time (SI Appendix, Fig. S7 A-F, panels i). We did not observe any alpha-helix formation and found instead that the mGluR3 CTD is conformationally dynamic with little or no regular secondary structure (SI Appendix, Fig. S7 A-F, panels ii), consistent with our CD data (*SI Appendix*, Fig. S2).

Our simulations consistently revealed conformations in which segments of the CTD were in contact with the membrane, especially in the N-terminal basic cluster region, where specific interactions between arginine residues and lipid headgroups were captured (Fig. 4A and Movies S1 and S2). To quantify such interactions, we analyzed hydrogen bonding between CTD sidechains and lipid headgroups over all of our simulations. We found that H-bonds between basic cluster arginine residues (R838 and R843) and PS headgroups anchor the N-terminal region to the membrane and that R869 also forms such H-bonds (Fig. 4B and SI Appendix, Fig. S8A). To more generally assess CTD-membrane interactions on a residue-by-residue basis, we calculated the distance of each sidechain in the CTD from the lipid phosphate plane. We find that when averaged over the individual replicas (SI Appendix, Fig. S7 A-F, panels iii) or over all the replicas (Fig. 4C) the N-terminal basic cluster region exhibits close proximity (≤10 Å) to the membrane surface, consistent with the tighter binding observed for this region in our NMR experiments. Time courses of arginine sidechain-phosphate plane distances for different trajectory segments reveal that R838 and R843 exhibit long periods of close proximity to the membrane (SI Appendix, Fig. S8 B and C), whereas R869 exhibits more dynamic behavior, suggesting that it mediates transient anchoring of the C-terminal portion of the CTD to the bilayer.

For the S/T-rich region, the distance distributions appear to be bimodal, with a minor population that is very close to the membrane surface and a larger population that is more distant. The membrane-proximal states may represent a bound population, which appears smaller than that observed by NMR for the anchored CTD peptide (SI Appendix, Fig. S6E), but unfortunately differences in the experimental and simulation conditions likely preclude a direct comparison. More generally, the simulations are consistent with the S/T-rich region binding the membrane less

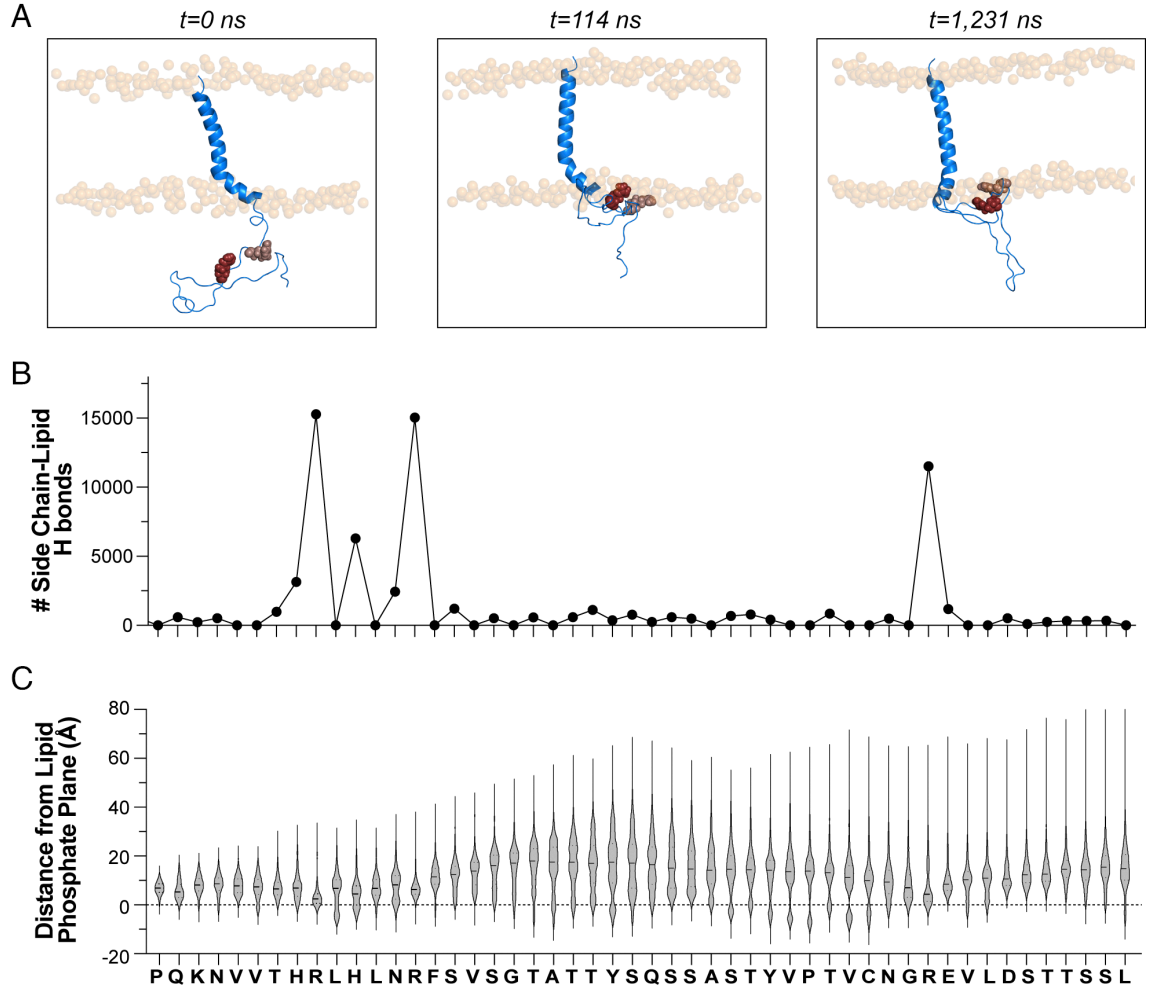


Fig. 4. Molecular dynamics simulations reveal multimodal membrane interactions of the intrinsically disordered mGluR3-CTD. (A) Snapshots of mGluR3 TM7-CTD (comprising TM7 residues 796-821 shown in cartoon helix representation, and CTD residues 822-879) replica 6 trajectory, highlighting three conformations of the CTD: the beginning of the simulation with no membrane contacts (t = 0, Left), and two membrane-associated states [t = 174.4 ns (Middle) and t = 1,231 ns (Right)]. Protein backbone is in blue cartoon; R838 (brown) and R843 (red) sidechains shown as spheres. (B) Total number of hydrogen bonds between each side chain and lipid headgroups averaged over all simulations. (C) Distributions, in the form of violin plots, of the distance of each residue (side chain center of mass) from the lipid phosphate plane over the course of all simulations (mean and quartiles depicted by solid and dotted horizontal lines, respectively).

tightly than the N-terminal basic cluster region, as indicated by our NMR data. Intriguingly, residue Y853 within the S/T-rich region (Fig. 5A), which we have shown confers β -arr-mediated internalization of mGluR3 (34), exhibits a population with negative distances from the lipid phosphate plane, indicating that its side chain inserts at least partially into the membrane. Aromatic residues are known to partition favorably into membranes and are often found in interfacial regions of TMDs (51–53). We examined the time course of the phosphate plane distance of Y853 and identified long (400 to 650 µs) time periods in separate replicas during which this distance was negative or very small (Fig. 5 B and C and SI Appendix, Fig. S8D). Individual poses of Y853 showed its sidechain inserted into the membrane or at the interfacial lipid headgroup region (Fig. 5B and Movies S1 and S2). Furthermore, the membrane proximity of nearby S/T residues appears to be correlated with that of Y853 (SI Appendix, Fig. S8E), while remaining dynamic (SI Appendix, Fig. S8F). To further probe the role of this aromatic residue in the membrane interactions of the S/T-rich region of the mGluR3 CTD, we examined the effects of mutating Y853 to alanine using our NMR-based assay. Compared to WT, Y853A resulted in a similar binding profile to 1:1 DOPC:DOPS vesicles for the N-terminal basic

region, but showed decreased binding of the CTD in the S/T-rich region (Fig. 5D and SI Appendix, Fig. S9 A and B). Indeed, the resulting profiles resemble those obtained at lower lipid concentrations (SI Appendix, Fig. S6A), indicating that Y853 helps to stabilize the membrane-bound state of the S/T-rich region that we observe at higher lipid concentrations.

Interestingly, the distance distributions of the C-terminal region of the CTD indicate that a hydrophobic region preceding residue R869 also features a population with negative distances from the membrane plane (Fig. 4C; residues Y861-C866). Although this is not strikingly evident in the NMR data, for both the unanchored (Fig. 2B) and anchored (SI Appendix, Fig. S6E) CTD, we observe a dip in the NMR intensity ratios in this region, and the NMR data for the anchored CTD show significant binding for the entire C-terminal region.

Noting that membrane-proximal conformations tended to be more extended in our simulations (Fig. 5B) we considered whether the radius of gyration (R_o) of CTD conformations correlated with membrane proximity. We observed a bimodal distribution of R_g in our simulations, with a pinch point around the average R, value of 15.5 Å (*SI Appendix*, Fig. S8*G*). We calculated the average distance from the membrane for the ensemble of conformations with $R_{\rm g}$

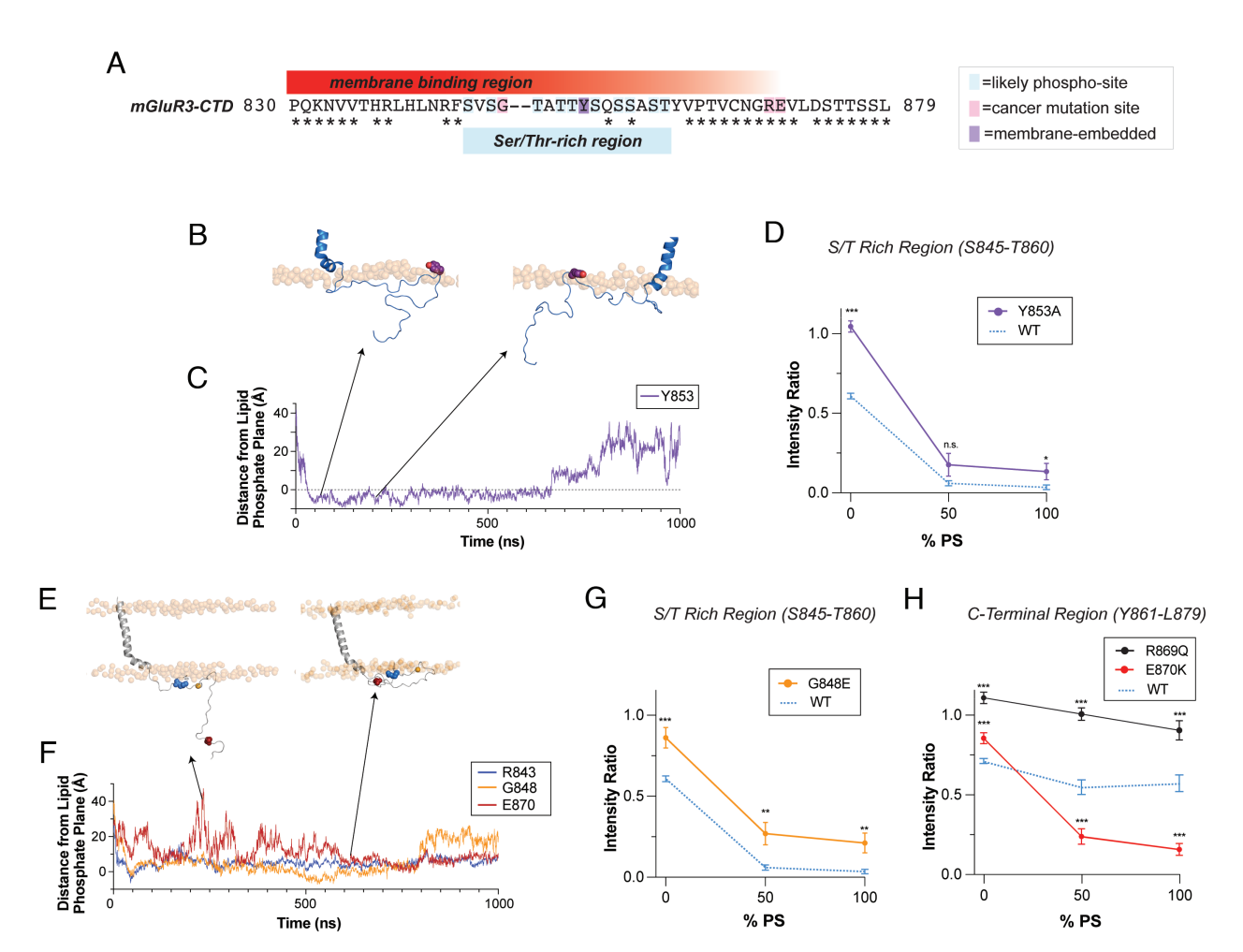


Fig. 5. Membrane interactions of the S/T-rich region of the mGluR3 CTD are modulated by mutation of a key residue and by cancer mutations. (A) mGluR3-CTD sequence annotated with the NMR- and MD-determined membrane-binding region and the overlapping Ser/Thr-rich region (* denotes residues conserved in mGluR2). (B) Snapshots of residue Y853 (shown as violet spheres with the hydroxyl group in red) in membrane-embedded and membrane-associated positions (from MD replica 6). Lipid phosphates are shown as transparent orange spheres. (C) Distance of Y853 sidechain to the lipid phosphate plane plotted as a function of time for MD replica 6 (first 1,000 ns). (D) Comparison of the averaged integrated NMR intensity ratios of WT (dotted blue) mGluR3-CTD (from Fig. 2B) with Y853A (purple) mGluR3-CTD (from SI Appendix, Fig. S9B) taken over the S/T-rich region (S845-T860) as a function of LUV lipid composition (±SEM of this average; Wilcoxon test; *P < 0.05, ***P < 0.001, n.s. $P \ge 0.05$). (E) Snapshots of residues R843 (blue), G848 (orange), and E870 (red) at different time points during the time course of MD replica 6 showing prolonged membrane-association of R843 and G848 and fluctuating membrane-association of E870 (protein backbone is in gray cartoon; side chains shown as spheres colored as in (F) below; lipid phosphates are shown as transparent orange spheres). (F) Position of side chains R843, G848, and E870 relative to the phosphate plane of the membrane (Methods) throughout the time course of MD replica 6. (G) Comparison of the averaged NMR intensity ratios of WT (dotted blue) mGluR3-CTD (from Fig. 2B) with G848E (orange) mGluR3-CTD (from *Sl Appendix*, Fig. S9B) taken over the S/T-rich region (S845-T860) as a function of LUV lipid composition (±SEM of this average; Wilcoxon test; **P < 0.01, ***P < 0.001). (H) Comparison of the averaged NMR intensity ratios of WT (dotted blue) mGluR3-CTD (from Fig. 2B) with R869Q (black) and E870K (red) mGluR3-CTD (from SI Appendix, Fig. S9B) taken over the last 19 residues (Y861-L879) as a function of LUV lipid composition (±SEM of this average; Wilcoxon test; ***P < 0.001).

below or above 15.5 Å and observed that conformations with lower R_g were biased toward shorter distances from the membrane (ŠI Appendix, Fig. S8H). We extended this analysis by separately considering, as a function of R_g, the distance of the N-terminal basic cluster region, the S/T-rich region, and the C-terminal region from the membrane. For the N-terminal region, the distance from the membrane was small (≤10 Å) irrespective of R_g, consistent with tight binding of this region to the membrane. For the S/T-rich and C-terminal regions, compact conformations were distributed closer to the membrane, while more extended conformations were distributed further from the membrane, consistent with more dynamic and reversible interactions with the membrane. These results, which can also be appreciated in Movies S1 and S2, suggest that membrane-binding restricts the conformational space of the CTD. Notably, both the S/T-rich and C-terminal regions featured a cluster of compact conformations situated very near (≤10 Å) the membrane surface, consistent with the sidechain-phosphate plane distance distributions (Fig. 4C).

CTD-Membrane Binding Is Modulated by Cancer-Associated Mutations. The mGluR3 CTD contains a number of cancerassociated mutations, two of which, G848E and E870K, are associated with melanomas (54) and a third, R869Q, which is enriched in carcinomas. While the role of these mutations in cancer remains unclear, each has been identified in multiple samples of cancer tissues (5, 4, and 6 samples for G848E, R869Q, and E870K) according to the COSMIC database (55). Multiple occurrences of identical mutations are statistically unlikely [estimated at 2E-12 for E870K (54)] and E870K has been also shown to increase melanoma cell growth, migration, and metastasis (54). Interestingly, each of these mutations alters the charge of the mGluR3 CTD, suggesting they could influence membrane interactions. G848 lies within the S/T-rich region, situated between R843 and Y853, and is membrane-associated according to both the NMR data and our MD simulations (Figs. 2B, 4C, and 5 E and F and Movies S3 and S4). R869 and E870 are in the C-terminal region of the mGluR3 CTD that is more weakly membrane associated according to the

NMR data and features transient contacts with the membrane in our simulations (Figs. 2B and 5 E and F and Movies S3 and S4). Based on these results, we hypothesized that these cancer-associated mutations could alter membrane binding due to changes in the local electrostatic properties of the mGluR3 CTD that would either diminish (G848E, R869Q) or promote (E870K) interactions with DOPS headgroups. To test this, we measured binding of these mutants using our NMR-based approach. The mGluR3 CTD G848E variant resulted in reduced interaction between the S/T-rich region of the CTD and the membrane, similar to the effect observed for the Y853A mutation (Fig. 5*G* and *SI Appendix*, Fig. S9 *A* and *B*). Strikingly, the R869Q mutation dramatically decreased membrane binding of both the S/T-rich region and of the C-terminal region of the CTD (Fig. 5*H* and *SI Appendix*, Fig. S9 *A* and *B*). In contrast, the E870K mutation extended the membrane-interacting region of the CTD nearly to its very C terminus (Fig. 5H and SI Appendix, Fig. S9 A and B). The ability of these cancer-associated mutations to alter CTD-membrane binding further supports the role of electrostatics in driving these interactions.

mGluR3 CTD Membrane Interactions Modulate Receptor Internalization in Living Cells. Having established that mGluR3 mutations can alter membrane binding in vitro, we next asked whether modifications which alter CTD-membrane interactions can also alter receptor function in living cells. We initially focused on agonist-induced mGluR3 internalization, which is driven by phosphorylation-dependent interactions with β -arrs (34). As described above, we reasoned that binding of the mGluR3 S/T-rich region to the membrane surface could modulate the ability of the CTD to interact with GRKs and/or β -arrs to mediate

We assessed the effects of the R843A, G848E, Y853A, R869Q, and E870K mutations (Fig. 6A) on mGluR3 internalization using an established live cell surface labeling imaging-based assay (34). All point mutants expressed on the surface, although a small decrease relative to wild type was observed for G848E (SI Appendix, Fig. S10A). To quantify receptor internalization, we labeled N-terminal SNAP-tagged mGluR3 transfected into HEK 293T cells with a membrane-impermeable fluorophore after 60 min treatment with agonist or antagonist. A consistent ~30% drop in fluorescence, reflecting receptor internalization, was observed for wild type mGluR3 following agonist treatment, reflecting endocytosis (Fig. 6B). Compared to WT, the R843A, G848E, Y853A, and R869Q mGluR3 mutants exhibit a greater degree of glutamate-evoked internalization (Fig. 6B). The data for G848E are consistent with our previous report that this mutation results in enhanced internalization (34). In contrast, the E870K mutation drastically decreased glutamate-induced internalization of mGluR3 (Fig. 6B). These results are consistent with our hypothesis that CTD-membrane interactions regulate the accessibility of the CTD to GRKs and β-arrs, with mutations that inhibit or enhance CTD-membrane binding exhibiting enhanced or blunted internalization, respectively.

To further assess our interpretation that altered CTD-membrane interactions underlie the observed changes in receptor internalization, we examined the effects of artificially anchoring the mGluR3 CTD to the membrane by appending a CAAX box lipidation motif to its C terminus (Fig. 6A and SI Appendix, Fig. S10A). Indeed, this variant exhibited a reduction in glutamate-induced receptor internalization similarly to the E870K mutant receptor (Fig. 6B). We also visualized receptor internalization via live cell microscopy where we labeled plasma membrane SNAP-tagged mGluR3 variants with a membrane-impermeable fluorophore and visualized fluorescence localization following

glutamate treatment (30 min, 1 mM). This analysis confirmed the enhanced internalization of R843A, G848E, Y853A, and R869Q and the reduced internalization of E870K and mGluR3-CAAX following glutamate treatment (SI Appendix, Fig. S10B).

To assess any effects of CTD mutations on G protein activation, we performed patch clamp measurements using a GIRK channel current assay (Methods). In this assay, R843A, G848E, and R869Q showed a clear left-shift while Y853A, E870K, and -CAAX did not show significantly different apparent glutamate affinities compared to wild type mGluR3 (Fig. 6C and SI Appendix, Fig. S10 C and D). These observations suggest that mutations can exert distinct functional effects on β-arr and G protein coupling.

Motivated by our observations of the contributions of residue Y853 to the membrane interactions of the mGluR3 CTD S/T-rich region, we posited that phosphorylation of this residue could influence CTD-effector interactions by reducing membrane binding. Consistent with this hypothesis, a phosphomimetic Y853D mutant showed enhanced internalization compared to WT (Fig. 6D) and also resulted in dramatically decreased membrane binding of the S/T-rich region (*SI Appendix*, Fig. S10*E*). We then found that treatment of mGluR3-transfected HEK 293T cells with epidermal growth factor (EGF; 100 ng/mL), which stimulates myriad downstream kinase signaling pathways, led to detectable internalization of WT, but not of Y853A mGluR3 in the absence of agonist (Fig. 6 E and F). Combining agonist and EGF treatment enhanced internalization to a similar extent to that observed for the agonist-treated Y853A mutant (Fig. 6B). Interestingly, the addition of EGFR tyrosine kinase inhibitor AG1478 eliminated EGF-induced internalization, while the application of Dasatinib, a pan-Src family tyrosine kinase inhibitor, did not produce a significant change in the EGF-induced internalization compared to the control (SI Appendix, Fig. S10H). This points toward a direct effect of the EGFR tyrosine kinase domain in either directly phosphorylating Y853 or activating a different downstream pathway that, ultimately, targets mGluR3. Together these results suggest that membrane-interacting residues in the mGluR3 CTD can contribute to both agonist-driven homologous internalization and heterologous internalization following stimulation of other cellular pathways.

In principle, the enhancement of mGluR3 internalization by Y853D could reflect increased binding to β-arr caused by mimicking phosphorylation within the S/T-rich region. The fact that Y853A also enhances internalization argues against this possibility, since it is unclear how the replacement of Y853 with an alanine would promote binding to β-arr. Nevertheless, we explored a subtler change at this position by replacing Y853 with phenylalanine. This mutation, which removes only one hydroxyl group, would not be expected to have a dramatic effect on any interaction with β-arr, but would be expected to enhance membrane binding by removing the polar hydroxyl group that restricts Y853 to the membrane interface region. Accordingly, we found that the Y853F mutation dramatically decreases receptor internalization (Fig. 6D). To verify the expected effect of this mutation on membrane binding, we examined binding at a series of lipid concentrations and showed that Y853F maintains strong binding of the S/T-rich region even at lower lipid concentrations, where binding by the WT CTD is decreased (*SI Appendix*, Fig. S6 *B* and *D*).

Discussion

The functional roles of disordered intracellular domains in GPCRs, particularly their CTDs, have drawn increasing interest in recent years. Several studies have confirmed the disordered nature of GPCR CTDs (3-6) and direct interactions of receptor

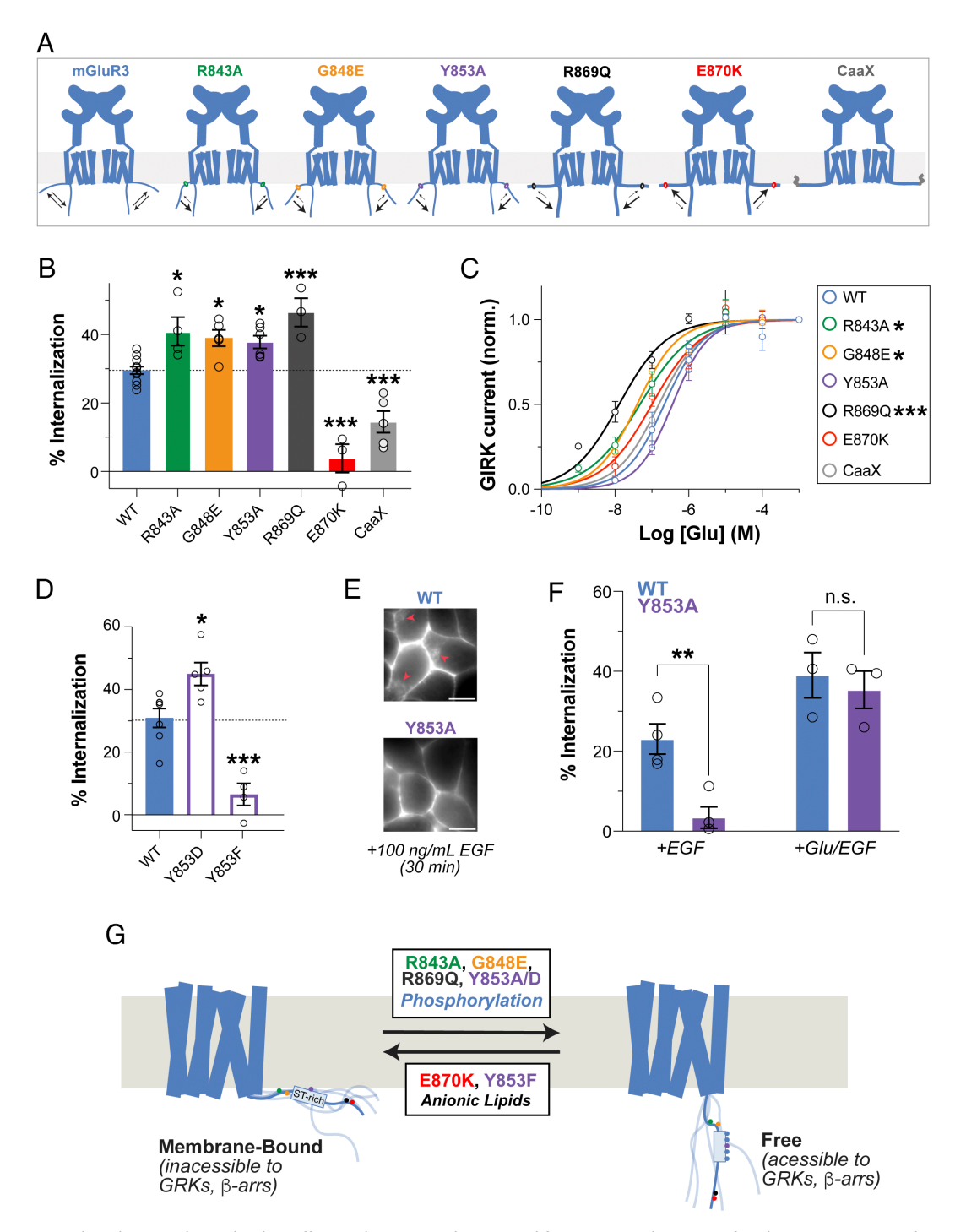


Fig. 6. CTD mutations that alter membrane binding affect mGluR3 internalization and function. (A) Schematics of mGluR3 CTD mutational positions and their effects on mGluR3-CTD free vs. membrane-bound equilibrium. Larger arrows show the direction in which each variant perturbs the equilibrium. (B) Quantification of the extent of receptor internalization for each mGluR3 variant (with dotted line denoting mGluR3 WT internalization) (averaged internalization per day, 10 to 12 images per condition/day and 4 to 9 d per condition; one-way ANOVA with multiple comparisons, *P < 0.05, ***P < 0.001). (C) Glutamate doseresponse curves for mGluR3 variants in a patch-clamp experiment using GIRK currents as a reporter for mGluR3 G-protein activation (EC50: WT = 137 ± 27 nM, R843A = 51 ± 12 nM, G848E = 44 ± 9 nM, Y853A = 418 ± 65 nM, R869Q = 14 ± 4 nM, E870K = 102 ± 22 nM, CAAX = 157 ± 43 nM; F-test of EC50 shifts; **P < 0.01, ***P < 0.001). (D) Quantification of the extent of receptor internalization of WT mGluR3 vs. Y853D phospho-mimetic mutant vs. Y853F (averaged internalization of 10 images per condition/day across 3 d; t test; *P < 0.05). (E) Representative images of HEK293T cells expressing SNAP-tagged mGluR3 WT vs Y853A treated with 100 ng/mL EGF for 30 min (red arrows represent internalization). (Scale bar, 5 μm.) (F) Quantification of the extent of internalization for mGluR3 WT vs Y853A mutant in EGF or Glu+EGF incubated conditions (averaged internalization per day, 10 images condition/day and 3 to 4 d per condition; t test, **P < 0.01, n.s. P ≥ 0.05). (G) Working model of mGluR3-CTD free vs. membrane-bound equilibrium and changes that favor the less accessible membrane-bound (E870K, Y853F, anionic lipids) or the more accessible free (R843A, G848E, R869Q, Y853A/D, phosphorylation) state.

CTDs with the intracellular face of the corresponding TMDs, which are regulated by phosphorylation and/or agonist binding and influence both receptor activity and coupling to β-arrs, have been documented (5, 6, 56). Direct membrane binding of disordered intracellular domains has been shown to play functional

roles for a number of membrane proteins (57–59), but GPCRs have not been the subject of such studies to date. Membrane phospholipid composition and cholesterol levels have been shown to modulate GPCR function (21, 22, 60), but this has been thought to occur primarily by direct interactions with membrane-embedded TMDs. Here, we show that family C GPCRs mGluR2 and mGluR3 can also sense the membrane in a functionally relevant way through their disordered intracellular CTDs, and that modulating CTD–membrane interactions alters receptor internalization.

We recently reported that mGluR3, but not mGluR2, couples strongly to β -arrs, dependent on the presence of an S/T-rich region in its CTD (34, 61). Here, we show that both CTDs are highly disordered in solution and bind to unilamellar lipid vesicles via their N-terminal regions. While many GPCRs feature a short amphipathic membrane-associated helix-8 (45), the mGluR2 and mGluR3 CTDs do not form detectable helical structure upon membrane binding. This is consistent with recently reported cryo-EM structures of full-length mGluR2 and mGluR3 which do not feature a classical helix 8 (9, 38, 62). Notably, our data do not rule out the possibility of very short helical segments in the membrane-bound CTDs, which have been observed in other intracellular membrane-binding domains (57).

We note precedents for IDP-membrane interaction modes that do not involve secondary structure formation, including the MARCKS-ED peptide from the effector domain of myristoylated alanine-rich C-kinase substrate (63, 64), which features 13 positively charged and 5 hydrophobic residues within a short 25-residue polypeptide segment. The C-terminal motif of worm complexin also binds to membranes without secondary structure via a combination of positively charged and hydrophobic side chains (47, 65). Another particularly relevant example is the N-terminal region of the Mycobacterium tuberculosis divisome protein ChiZ, which binds to acidic membranes primarily via hydrogen bonds between phospholipid headgroups and 9 arginine

We posit that CTD-membrane interactions can regulate CTD availability for interactions with downstream effectors such as GRKs and β -arrs (Fig. 6G). We demonstrated that mutations that reduce membrane association (R843A, G848E, Y853A, Y853D, and R869Q) result in increased receptor internalization, whereas mutations or modifications that enhance membrane binding (Y853F, E870K, and introduction of a CAAX box motif) result in decreased receptor internalization. Importantly, half of these modifications are distant from the S/T-rich region of mGluR3 and are therefore unlikely to directly impact binding to GRKs or β -arrs. The presence of Y853 within the S/T-rich region and its importance for the membrane interactions of this region prompted us to hypothesize that phosphorylation of this tyrosine residue could also modulate CTD-membrane binding and thereby regulate coupling to transducers, including β -arrs. Notably, tyrosine phosphorylation has been reported to disrupt localized membrane binding of several disordered proteins (67, 68). While not providing direct proof, the dependence of EGF-induced mGluR3 internalization on the presence of Y853 and its elimination by an EGF kinase inhibitor support this possibility, as does the enhanced internalization we observe for the phosphomimetic Y853D mutation. This would also be consistent with literature reports of heterologous receptor internalization/desensitization (69). Alternative explanations may exist and could include EGFR activation of GRK2 and downstream Ser/Thr phosphorylation in the CTD (70), but it is unclear how this could account for the requirement for Y853. In light of our observations and of previous reports of the role of tyrosine-membrane interactions in regulating T cell receptor activation (57), we posit that modulation of such interactions, either directly by phosphorylation or indirectly by other mechanisms may constitute a general mechanism for receptor regulation.

The work presented here makes a case for a general role for GPCR CTD-membrane nteractions in regulating the accessibility of receptor CTDs to downstream effectors, including β -arrs (Fig. 6G). An appealing aspect of this model is that it provides a mechanism for sequential or cooperative phosphorylation (71) as initial phosphorylation events could shift the equilibrium of phosphocode-containing regions (14, 72) and increase their accessibility for further phosphorylation and subsequent β-arr binding. Together with recent results describing functionally important interactions of receptor CTDs with the intracellular face of their TMDs (5, 6, 56), our work expands the modalities by which GPCR CTDs can regulate receptor function. Important questions remain regarding how the interplay of CTD interactions with membranes, TMDs, G-proteins, GRKs, β-arrs and other effectors is regulated and orchestrated. Mutations that alter CTD-membrane interactions could also affect direct CTD G-protein binding/recruitment (7-9), autoinhibitory CTD interactions with G-protein binding sites on the TMD (5, 34, 56), or allosteric effect on TMD conformation, especially since these other interactions may also include electrostatic components. Indeed, we observe that mutations that strongly disrupt CTD-membrane binding facilitate receptor activation and we also recently reported an autoinhibitory effect of the mGluR2 CTD on β-arr coupling (34), supporting a potential interplay between G-protein, TMD, and membrane binding. Recent studies of the calcium-sensing receptor (CaSR) also proposed a potential interplay between sequestration of a short CTD segment and its interactions with G-proteins (73). While our focus here has been on the CTD, similar mechanisms and interactions may be operative for other disordered intracellular GPCR domains (74).

Conclusions

Our results establish a previously unappreciated yet critical and dynamic role of CTD membrane interactions in controlling GPCR desensitization and internalization and suggest that an equilibrium between membrane-bound and free states controls transducer coupling efficiency. This equilibrium may be modified in multiple ways, including disease mutations, Ser/Thr phosphorylation, and possibly Tyr phosphorylation, as well as changes in membrane composition, comprising an additional mode of CTD-mediated GPCR regulation.

Methods

Recombinant proteins were expressed in bacteria as fusion proteins and purified by affinity chromatography. LUVs were prepared from the appropriate lipid composition by extrustion. NMR 2D experiments were collected at 500 MHz and triple-resonance experiments for assignments were collected at 800 MHz. CD measurements were performed on an AVIV 410 CD spectropolarimeter over a wavelength range from 300 to 190 nm. MD simulations of an mGluR3 construct containing both TM7 and the CTD (residues 796-879) used initial poses generated using AlphaFold2 (75) and ColabFold (76) which were equilibrated using the standard CHARMM-GUI-based protocol and scripts followed by a short, 6-ns run using OpenMM (77) and the CHARMM36m (78) forcefield and then simulated for 1,370 ns for each of six replicas. Whole-cell patch clamp recordings were performed in HEK 293 cells 24 h posttransfection as previously described (79). For quantifying receptor internalization we used a previously reported surface labeling assay (34). Details of all methodologies applied in this study are included in SI Appendix.

Data, Materials, and Software Availability. All NMR chemical shift assignments can be obtained online from the biological magnetic resonance database (BMRB Accession Nos. 52206 (80) and 52202 (81). NMR intensity ratio data, CD data, MD trajectories, and all code used for the analysis of MD simulations can be obtained online at GitHub (https://github.com/cmanci/mGluR_CTD) (82). Imaging data, as well as all plasmids and reagents used in the study, will be made available upon request to the corresponding authors.

ACKNOWLEDGMENTS. This work was funded in part by NIH Grants R35GM136686 (D.E.), R01NS129904 (J.L.), F32GM148001 (D.C.M.), and F31AG077836 (C.D.M.) and the Margarita Salas Fellowship from the Ministry of Universities of Spain (A.J.G.-H), the Rohr Family Research Scholar Award (J.L.), and the Monique Weill-Caulier Award (J.L.). G.K. gratefully acknowledges support from the 1923 Fund. The WCM NMR core is supported by NIH shared Instrumentation Grants S100D028556 and S100D016320. We acknowledge assistance from Clay Bracken and Emily Grasso with NMR data collection and processing, Jihye Kim for guidance on EGF stimulation studies and Derek Shore for assistance setting up simulations. We gratefully acknowledge the use of in-house computational resources of the David A. Cofrin Center for Biomedical Information in the Institute for Computational Biomedicine at Weill Cornell Medical College.

Author affiliations: ^aDepartment of Biochemistry, Weill Cornell Medicine, New York, NY 10065; ^bDepartment of Physiology and Biophysics, Weill Cornell Medicine, New York, NY 10065; ^cDepartment of Psychiatry, Weill Cornell Medicine, New York, NY 10065; and ^dBrain and Mind Research Institute, Weill Cornell Medicine, New York, NY 10065

Author contributions: C.D.M., D.C.M., A.J.G.-H., G.K., J.L., and D.E. designed research; C.D.M., D.C.M., A.J.G.-H., K.H., L.M., and A.A. performed research; C.D.M., D.C.M., and A.J.G.-H. contributed new reagents/analytic tools; C.D.M., D.C.M., A.J.G.-H., J.L., and D.E. analyzed data; and C.D.M., D.C.M., A.J.G.-H., G.K., J.L., and D.E. wrote the paper.

- D. Wacker, R. C. Stevens, B. L. Roth, How ligands illuminate GPCR molecular pharmacology. Cell 170, 414-427 (2017).
- K. Sriram, P. A. Insel, G protein-coupled receptors as targets for approved drugs: How many targets and how many drugs? Mol. Pharmacol. 93, 251-258 (2018).
- M. Guillien et al., Structural insights into the intrinsically disordered GPCR C-terminal region. Major actor in Arrestin-GPCR interaction, Biomolecules 12, 617 (2022).
- M. Guillien et al., Phosphorylation motif dictates GPCR C-terminal domain conformation and arrestin interaction. bioRxiv [Preprint] (2023). https://doi.org/10.1101/2023.02.23.529712 (Accessed 6 May 2024).
- J. Heng et al., Function and dynamics of the intrinsically disordered carboxyl terminus of beta2 5 adrenergic receptor. Nat. Commun. 14, 2005 (2023).
- Y. Shiraishi et al., Phosphorylation-induced conformation of beta(2)-adrenoceptor related to arrestin recruitment revealed by NMR. Nat. Commun. 9, 194 (2018).
- S. Maeda, Q. Qu, M. J. Robertson, G. Skiniotis, B. K. Kobilka, Structures of the M1 and M2 muscarinic acetylcholine receptor/G-protein complexes. Science 364, 552-557 (2019).
- C. J. Tsai et al., Cryo-EM structure of the rhodopsin-Galphai-betagamma complex reveals binding of the rhodopsin C-terminal tail to the gbeta subunit. eLife 8, e46041 (2019).
- A. B. Seven et al., G-protein activation by a metabotropic glutamate receptor. Nature 595, 450-454 (2021).
- F. He et al., Allosteric modulation and G-protein selectivity of the Ca(2+)-sensing receptor. Nature 10 626. 1141-1148 (2024).
- O. G. Kisselev, J. H. McDowell, P. A. Hargrave, The arrestin-bound conformation and dynamics of the
- phosphorylated carboxy-terminal region of rhodopsin. FEBS Lett. **564**, 307–311 (2004).

 A. K. Shukla *et al.*, Structure of active beta-arrestin-1 bound to a G-protein-coupled receptor phosphopeptide. Nature 497, 137-141 (2013).
- K. Min et al., Crystal structure of beta-arrestin 2 in complex with CXCR7 phosphopeptide. Structure 28, 1014-1023.e1014 (2020).
- X. E. Zhou et al., Identification of phosphorylation codes for arrestin recruitment by G proteincoupled receptors. Cell 170, 457-469.e413 (2017).
- W. Yin et al., A complex structure of arrestin-2 bound to a G protein-coupled receptor. Cell Res. 29,
- 16. D. P. Staus et al., Structure of the M2 muscarinic receptor-beta-arrestin complex in a lipid nanodisc. Nature 579, 297-302 (2020).
- W. Huang et al., Structure of the neurotensin receptor 1 in complex with beta-arrestin 1. Nature **579**, 303-308 (2020).
- K. H. Ahn et al., Structural analysis of the human cannabinoid receptor one carboxyl-terminus 18. identifies two amphipathic helices. Biopolymers 91, 565-573 (2009).
- A. Patwardhan, N. Cheng, J. Trejo, Post-translational modifications of G protein-coupled receptors control cellular signaling dynamics in space and time. Pharmacol. Rev. 73, 120-151 (2021).
- 20 W. Song, H. Y. Yen, C. V. Robinson, M. S. P. Sansom, State-dependent lipid interactions with the A2a receptor revealed by MD simulations using in vivo-mimetic membranes. Structure 27, 392-403.
- R. Dawaliby et al., Allosteric regulation of G protein-coupled receptor activity by phospholipids. Nat. Chem. Biol. 12, 35-39 (2016).
- H. Y. Yen et al., PtdIns(4,5)P2 stabilizes active states of GPCRs and enhances selectivity of G-protein coupling. Nature 559, 423-427 (2018).
- J. Janetzko et al., Membrane phosphoinositides regulate GPCR-beta-arrestin complex assembly and dynamics. Cell 185, 4560-4573.e4519 (2022).
- M. Guillien et al., Phosphorylation motif dictates GPCR C-terminal domain conformation and arrestin interaction. Structure 31, P1394-1406.E7 (2023).
- Q. Chen et al., ACKR3-arrestin2/3 complexes reveal molecular consequences of GRK-dependent barcoding. bioRxiv [Preprint] (2023). https://doi.org/10.1101/2023.07.18.549504 (Accessed 6 May
- A. Ellaithy, J. Gonzalez-Maeso, D. A. Logothetis, J. Levitz, Structural and biophysical mechanisms of 26 class C G protein-coupled receptor function. Trends Biochem. Sci. 45, 1049-1064 (2020).
- A. S. Dore et al., Structure of class C GPCR metabotropic glutamate receptor 5 transmembrane domain. Nature 511, 557-562 (2014).
- 28 H. Wu et al., Structure of a class C GPCR metabotropic glutamate receptor 1 bound to an allosteric modulator. Science 344, 58-64 (2014).
- J. Du et al., Structures of human mGlu2 and mGlu7 homo- and heterodimers. Nature 594, 589-593
- R. Enz, Structure of metabotropic glutamate receptor C-terminal domains in contact with interacting proteins. Front Mol. Neurosci. 5, 52 (2012).
- A. Reiner, J. Levitz, Glutamatergic signaling in the central nervous system: lonotropic and metabotropic receptors in concert. Neuron 98, 1080-1098 (2018).
- J. P. Pin, B. Bettler, Organization and functions of mGlu and GABA(B) receptor complexes. Nature 32. **540**, 60-68 (2016).
- Y. H. Suh, K. Chang, K. W. Roche, Metabotropic glutamate receptor trafficking. Mol. Cell Neurosci. 91, 33 10-24 (2018)
- N. Abreu, A. Acosta-Ruiz, G. Xiang, J. Levitz, Mechanisms of differential desensitization of metabotropic glutamate receptors. Cell Rep. 35, 109050 (2021).

- 35. S. Lin et al., Structures of G(i)-bound metabotropic glutamate receptors mGlu2 and mGlu4. Nature **594**, 583-588 (2021).
- A. Koehl et al., Structural insights into the activation of metabotropic glutamate receptors. Nature 566, 79-84 (2019).
- 37. C. Nasrallah et al., Agonists and allosteric modulators promote signaling from different metabotropic glutamate receptor 5 conformations. Cell Rep. 36, 109648 (2021).
- A. Strauss et al., Structural basis of allosteric modulation of metabotropic glutamate receptor activation and desensitization. bioRxiv [Preprint] (2023). https://doi. org/10.1101/2023.08.13.552748 (Accessed 6 May 2024).
- T. Das, D. Eliezer, Membrane interactions of intrinsically disordered proteins: The example of alphasynuclein. Biochim. Biophys. Acta Proteins Proteom. 1867, 879–889 (2019).
- T. Das, D. Eliezer, Probing structural changes in alpha-synuclein by nuclear magnetic resonance spectroscopy. Methods Mol. Biol. 1948, 157-181 (2019).
- D. Snead, D. Eliezer, Spectroscopic characterization of structure-function relationships in the intrinsically disordered protein complexin. Methods Enzymol. 611, 227-286 (2018).
- W. Parker, P. S. Song, Protein structures in SDS micelle-protein complexes. Biophys. J. 61, 1435-1439 (1992).
- R. Bussell Jr., D. Eliezer, A structural and functional role for 11-mer repeats in alpha-synuclein and other exchangeable lipid binding proteins. J. Mol. Biol. 329, 763-778 (2003).
- D. Snead et al., Unique structural features of membrane-bound C-terminal domain motifs modulate complexin inhibitory function. Front Mol. Neurosci. 10, 154 (2017).
- P. M. Dijkman et al., Conformational dynamics of a G protein-coupled receptor helix 8 in lipid membranes. Sci. Adv. 6, eaav8207 (2020).
- J. T. Nielsen, F. A. A. Mulder, CheSPI: Chemical shift secondary structure population inference. J. Biomol. NMR 75, 273-291 (2021).
- D. Snead, R. T. Wragg, J. S. Dittman, D. Eliezer, Membrane curvature sensing by the C-terminal domain of complexin. Nat. Commun. 5, 4955 (2014).
- B. Antonny, Mechanisms of membrane curvature sensing. Annu. Rev. Biochem. 80, 101-123
- H. I. Ingolfsson et al., Lipid organization of the plasma membrane. J. Am. Chem. Soc. 136, 14554-14559 (2014).
- M. Klahn, M. Zacharias, Transformations in plasma membranes of cancerous cells and resulting consequences for cation insertion studied with molecular dynamics. Phys. Chem. Chem. Phys. 15, 14427-14441 (2013).
- 51. S. K. McDonald, K. G. Fleming, Aromatic side chain water-to-lipid transfer free energies show a depth dependence across the membrane normal. J. Am. Chem. Soc. 138, 7946-7950 (2016).
- C. P. Moon, K. G. Fleming, Side-chain hydrophobicity scale derived from transmembrane protein folding into lipid bilayers. Proc. Natl. Acad. Sci. U.S.A. 108, 10174-10177 (2011).
- J. A. Killian, G. von Heijne, How proteins adapt to a membrane-water interface. Trends Biochem. Sci. 25, 429-434 (2000).
- T. D. Prickett et al., Exon capture analysis of G protein-coupled receptors identifies activating mutations in GRM3 in melanoma. Nat. Genet 43, 1119-1126 (2011).
- Z. Sondka et al., COSMIC: A curated database of somatic variants and clinical data for cancer. Nucleic Acids Res. 52, D1210-D1217 (2024).
- W. B. Asher et al., GPCR-mediated beta-arrestin activation deconvoluted with single-molecule precision. Cell 185, 1661-1675 e1616 (2022).
- C. Xu et al., Regulation of T cell receptor activation by dynamic membrane binding of the CD3epsilon cytoplasmic tyrosine-based motif. Cell 135, 702-713 (2008).
- Y. Wang et al., Regulation of EGFR nanocluster formation by ionic protein-lipid interaction. Cell Res. 24, 959-976 (2014).
- J. Cornish, S. G. Chamberlain, D. Owen, H. R. Mott, Intrinsically disordered proteins and membranes: A marriage of convenience for cell signalling? *Biochem. Soc. Trans.* **48**, 2669–2689 (2020).
- 60. I. Menon et al., A cholesterol switch controls phospholipid scrambling by G protein-coupled receptors. J. Biol. Chem. 300, 105649 (2024).
- $\label{eq:conditional} \textbf{J}. \textbf{Lee} \textit{ et al., } \textbf{Distinct beta-arrestin coupling and intracellular trafficking of metabotropic glutamate}$ receptor homo- and heterodimers. Sci. Adv. 9, eadi8076 (2023).
- W. Fang et al., Structural basis of the activation of metabotropic glutamate receptor 3. Cell Res. 32, 695-698 (2022).
- L. A. Morton et al., MARCKS-ED peptide as a curvature and lipid sensor. ACS Chem. Biol. 8, 218-225
- J. Wang et al., Lateral sequestration of phosphatidylinositol 4,5-bisphosphate by the basic effector domain of myristoylated alanine-rich C kinase substrate is due to nonspecific electrostatic interactions. J. Biol. Chem. 277, 34401-34412 (2002).
- R. T. Wragg et al., Evolutionary divergence of the C-terminal domain of complexin accounts for functional disparities between vertebrate and invertebrate complexins. Front. Mol. Neurosci. 10, 146 (2017).
- A. Hicks, C. A. Escobar, T. A. Cross, H. X. Zhou, Fuzzy association of an intrinsically disordered protein with acidic membranes. JACS Au 1, 66-78 (2021).
- I. Dikiy et al., Semisynthetic and in vitro phosphorylation of alpha-synuclein at Y39 promotes functional partly helical membrane-bound states resembling those induced by PD mutations. ACS Chem. Biol. 11, 2428-2437 (2016).

- 68. D. M. Acosta, C. Mancinelli, C. Bracken, D. Eliezer, Post-translational modifications within tau paired helical filament nucleating motifs perturb microtubule interactions and oligomer formation. J. Biol. Chem. 298, 101442 (2022).
- L. E. Kilpatrick, S. J. Hill, Transactivation of G protein-coupled receptors (GPCRs) and receptor tyrosine kinases (RTKs): Recent insights using luminescence and fluorescence technologies. Curr. Opin. Endocr. Metab. Res. 16, 102-112 (2021).
- Y. Chen, H. Long, Z. Wu, X. Jiang, L. Ma, EGF transregulates opioid receptors through EGFR-mediated GRK2 phosphorylation and activation. Mol. Biol. Cell 19, 2973–2983 (2008).
- 71. A. B. Tobin, G-protein-coupled receptor phosphorylation: Where, when and by whom. Br. J. Pharmacol. 153, S167-S176 (2008).
- 72. K. N. Nobles et al., Distinct phosphorylation sites on the beta(2)-adrenergic receptor establish a barcode that encodes differential functions of beta-arrestin. Sci. Signal. 4, ra51 (2011).
- Y. Gao et al., Asymmetric activation of the calcium-sensing receptor homodimer. Nature 595, 455-459 (2021).
- K. Pluhackova, F. M. Wilhelm, D. J. Muller, Lipids and phosphorylation conjointly modulate complex formation of beta(2)-adrenergic receptor and beta-arrestin2. Front. Cell Dev. Biol. 9, 807913 (2021).

- 75. J. Jumper et al., Highly accurate protein structure prediction with AlphaFold. Nature 596, 583-589
- M. Mirdita et al., ColabFold: Making protein folding accessible to all. Nat. Methods 19, 679-682 (2022).
- P. Eastman et al., OpenMM 7: Rapid development of high performance algorithms for molecular dynamics. PLoS Comput. Biol. 13, e1005659 (2017).
- 78. J. Huang et al., CHARMM36m: An improved force field for folded and intrinsically disordered proteins. Nat. Methods 14, 71-73 (2017).
- V. A. Gutzeit et al., A fine-tuned azobenzene for enhanced photopharmacology in vivo. Cell Chem. Biol. 28, 1648-1663.e1616 (2021).
- C. D. Mancinelli et al., Rat metabatropic glutamate receptor 2 WT C-terminal domain. BMRB. https://dev.bmrb.io/data_library/summary/index.php?bmrbId=52206. Deposited 10 November 2023.
- C. D. Mancinelli et al., Rat metabatropic glutamate receptor 3 WT C-terminal domain. BMRB. https://bmrb.io/data_library/summary/?bmrbId=52202. Deposited 9 November 2023.
 C. D. Mancinelli et al., Cmanci/mGluR_CTD. GitHub. https://github.com/cmanci/mGluR_CTD.
- Deposited 7 May 2024.